



Combining functional, structural, and morphological networks for multimodal classification of developing autistic brains

Changchun He^{1,3,4,8} · Jesus M. Cortes^{5,9,10} · Yi Ding⁴ · Xiaolong Shan^{2,7} · Maoyang Zou^{1,8} · Heng Chen⁶ · Huafu Chen^{2,7} · Xianmin Wang³ · Xujun Duan^{2,7}

Accepted: 17 May 2025

© The Author(s), under exclusive licence to Springer Science+Business Media, LLC, part of Springer Nature 2025

Abstract

Accumulating neuroimaging evidence suggests that abnormal functional and structural brain connectivity plays a cardinal role in the pathophysiology of autism spectrum disorder (ASD). Here, we constructed brain networks of functional, structural, and morphological connectivity using data from functional magnetic resonance imaging (fMRI), diffusion tensor imaging (DTI), and structural magnetic resonance imaging (sMRI), respectively. The neuroimaging data from a cohort of 50 individuals with ASD and 47 age-, gender- and handedness-matched TDC (age range: 5–18 years) were selected from the Autism Brain Image Data Exchange database. The combination of the fMRI, sMRI and DTI modalities connectivity features resulted in a classification accuracy of 82.69% for differentiating individuals with ASD from TDC. This accuracy surpassed that of any single modality or combination of fMRI and DTI modalities previously examined. Among the fMRI, sMRI and DTI modalities, the most distinguishing connectivity features were observed in the temporal, parietal, and occipital lobes from the DTI modality, the prefrontal and parietal lobes from the fMRI modality, and the temporal lobe from the sMRI modality. In addition, we also found that these distinguishing connectivity features can predict abnormal social interaction behaviours in ASD. These results highlight the complementary information provided by multimodal approaches, further emphasizing the pivotal role of multimodal connectivity patterns in unravelling the intricate mechanisms involved in the pathophysiology of ASD.

Keywords Magnetic resonance imaging · Classification · Brain network · Multi-modality · Autism

✉ Changchun He
changchunhh@gmail.com

✉ Huafu Chen
chenhf@uestc.edu.cn

✉ Xianmin Wang
wxm6910@163.com

✉ Xujun Duan
duanxujun@uestc.edu.cn

¹ College of Artificial Intelligence (CUIT Shuangliu Industrial College), Chengdu University of Information Technology, Chengdu 610225, China

² MOE Key Lab for Neuroinformation, High-Field Magnetic Resonance Brain Imaging Key Laboratory of Sichuan Province, University of Electronic Science and Technology of China, Chengdu 610054, PR China

³ Sichuan Provincial Women's and Children's Hospital, Affiliated Women's and Children's Hospital of Chengdu Medical College, Chengdu 610045, PR China

⁴ Network and Data Security Key Laboratory of Sichuan Province, School of Information and Software Engineering, University of Electronic Science and Technology of China, Chengdu 610054, China

⁵ Department of Cell Biology and Histology, University of the Basque Country, Leioa, Spain

⁶ Medical College of Guizhou University, Guiyang 550025, PR China

⁷ The Clinical Hospital of Chengdu Brain Science Institute, School of Life Science and Technology, University of Electronic Science and Technology of China, Chengdu 610054, PR China

⁸ National Intelligent Society Comprehensive Governance Experimental Base (CUIT Shuangliu Industrial College), Chengdu 610225, China

⁹ Biocruces-Bizkaia Health Research Institute, Barakaldo, Spain

¹⁰ Ikerbasque: The Basque Foundation for Science, Bilbao, Spain

Introduction

Autism spectrum disorder (ASD) is a condition with a neurodevelopmental origin that causes challenges in social communication, social reciprocity, and repetitive and stereotyped behaviors and interests (Association American Psychiatric, 2013). Currently, the clinical recognition of ASD has focused on understanding its neurobiological foundations involved in inter-regional communication in the brain development process (Uddin et al., 2013). Numerous functional magnetic resonance imaging (fMRI) studies have identified the prevailing notion that individuals with ASD have abnormally increased connectivity under the age of 12 but decreased connectivity and possibly degenerates in adolescence (Courchesne et al., 2007; He et al., 2020; Uddin et al., 2013). Diffusion tensor imaging (DTI) has also verified that the altered FA values in individuals with ASD are age-related, and further reported increased FA values in young children with ASD and decreased FA values in adolescents or adults with ASD (Alexander et al., 2007; Bashat et al., 2007; Keller et al., 2007). Additionally, structural MRI (sMRI) studies have suggested that numerous brain regions undergo a period of precocious growth during early postnatal life followed by a deceleration in age-related growth in autistic brains, and these regions form an integrated structural network (Courchesne et al., 2003). These autistic studies demonstrated that abnormal brain connectivity patterns are relatively remarkable in the developmental period. Previous studies from our group have also shown that morphological connectivity abnormalities can predict the severity of social communication deficits in young children with ASD, thus confirming an associational impact at the behavioral level (He et al., 2021). Therefore, considering the association of behavioral deficits with abnormal neuro-anatomical connectivity and its functional consequences in developing autistic brains, measures of brain connectivity associated with symptom severity are promising biomarkers for ASD diagnosis (Jeste et al., 2015).

Recent research has verified that structural connectivity provides support to functional connectivity, while functional connectivity follows the plasticity of structural connectivity in the course of brain development (Diez et al., 2015; Hermundstad et al., 2013; Rasero et al., 2023). Moreover, many studies have demonstrated large spatial resemblances of the connectivities between fMRI and DTI modalities within the whole-brain large-scale network. Recently, the coupling of functional and structural connectivity networks has been detected to increase with age and to be disturbed in disease-specific states. Heretofore, the important limitations of solely relying on a single connectivity modality were always reported to investigate the neurobiological foundations of ASD. For example, functional network analyses are

known to be highly sensitive to physiological noise and head motion (Reid et al., 2016), which can result in an excess of systemic false correlations in ASD. Structural network analyses in ASD (Cheng et al., 2010) have very often used deterministic tractography algorithms to construct structural connectivity networks. Although such calculations can be performed quickly, they do not address the issue of fiber crossing. Morphological gray matter networks have also provided valuable information regarding the coordination of gray matter growth/ atrophy (Evans, 2013; Fox, 2018). Recently, Keller et al. found that the reduction in the structural integrity of white matter may underlie functional connectivity alterations, which may be responsible for some of the social and cognitive symptoms found in ASD, including deficits in the ‘theory of mind’ (Baron-Cohen et al., 1985; Keller et al., 2007). Overall, the combination of different modalities of brain connectivity in autistic brains may alleviate their single-modality weakness and further provide comprehensive and complementary information (Zhao et al., 2020).

Some researchers studying ASD have recently begun to incorporate two or three imaging techniques. For instance, Rakic et al. have reported that the classification model with the features based on fMRI and sMRI modalities outperforms that with implemented individual pipelines (Rakić et al., 2020). Furthermore, many studies have reported that integrating fMRI, DTI and Electroencephalogram (EEG) sources helps allow a comprehensive and personalized computer-aided diagnostic for autistic patients (Cociu et al., 2017; ElNakieb et al., 2018). However, they do not make complete use of three-modal (including fMRI, sMRI and DTI modalities) brain connectivity features, which can provide more communication information among brain regions. This study provides answers to the following two questions: (a) whether the biomarkers discovered via combining fMRI, sMRI and DTI modalities can reliably discriminate autistic individuals and further improve the classification accuracy compared with those based on the single modality (i.e., fMRI, sMRI, or DTI modality) or two modalities (including fMRI+DTI, fMRI+sMRI, or DTI+sMRI); and (b) whether there were any associations between symptoms severity in ASD and biomarkers discovered via different modalities.

Materials and methods

Participants

All data were obtained from the public dataset (Autism Brain Imaging Data Exchange (ABIDE II) repository, https://fcon_1000.projects.nitrc.org/indi/abide/) (Di Martino et al., 2014, 2017), based on stringent inclusion criteria. The

inclusion criteria were as follows: (a) high-quality images within sMRI, resting-state fMRI, and DTI dataset; (b) age ranging from 5 to 18; (c) head motion less than 3 mm translation or 3° angular rotation in any direction; (d) scanning sites with more than 10 subjects. After applying these selection criteria, the final dataset for this study comprised 47 TDC and 50 ASD individuals, collected from two research scanning sites (New York University Langone Medical Center [NYU] and San Diego State University [SDSU]). Subjects were also fully anonymized using the Health Insurance Portability and Accountability Act (HIPAA) guidelines. Written consent was obtained from the parents or legal representatives. This study was approved by the institutional review boards of the New York University and the San Diego State University Institutional Review Boards.

Diagnosis and clinical assessment

Participants with ASD were diagnosed following the DSM-IV-TR criteria, through a series of differentiated clinical diagnoses, including Autistic Disorder Asperger's Disorder, or Pervasive Developmental Disorder Not-Otherwise-Specified, the Autism Diagnostic Observation Schedule, ADOS, and/or the Autism Diagnostic Interview-Revised, ADI-R (Detailed information is provided in https://fcon_1000.projects.nitrc.org/indi/abide/abide_II.html). In the NYU and SDSU datasets, participants had no co-morbid Fragile-X or tuberous sclerosis. Intelligence (full scale IQ, performance IQ, and verbal IQ) was measured by the Wechsler Abbreviated Scale of Intelligence (WASI) or the six subtests of the Differential Ability Scales, Second Edition (DAS-II). TDC had no history of mental disorders.

Neuroimaging acquisition

Magnetic resonance imaging (MRI) data were acquired at the NYU Langone Medical Center using a 3 Tesla Siemens Magnetom Allegra syngo MR 2004 A (Spisak et al., 2014). Resting-state fMRI images were obtained using the following acquisition parameters: repetition time/echo time (TR/TE)=2000/15 ms, 33 slices, 90° flip angle, voxel size=3×3×4 mm³, field of view (FOV)=240×192 mm², and slice thickness=4.0 mm. For each subject, the scanning time lasted for 6 min and 180 volumes were obtained (Guo et al., 2017). T1-weighted sagittal MP-RAGE structural images were acquired using gradient echo sequence with the following parameters: TR/TE=2530/3.25 ms, TI=1100 ms, 7° flip angle, matrix size=256×256, FOV=256 mm, slice thickness=1.33 mm, 128 sagittal slices with 1.3×1.0×1.3 mm³ voxels (Koyama et al., 2013). DTI scans were collected using a twice-refocused diffusion-weighted echo-planar image sequence with the following parameters: TR/TE=5200/78

ms, acquisition matrix=64×64, FOV=192×192 mm², 50 slices with 3×3×3 mm³ voxel, $b=0$ and 1000 s/mm² along 64 non-collinear directions (Yoncheva et al., 2016).

MRI data at SDSU were acquired on a 3 Tesla GE MR750 scanner using an echo-planar imaging (EPI) sequence with whole-brain coverage. Resting-state fMRI images were obtained using the following acquisition parameters: TR/TE=2000/30 ms, 42 slices with 3.4×3.4×3.4 mm³, 90° flip angle, FOV=220×220 mm², slice thickness=3.4 mm. For each subject, 180 volumes were collected over an fMRI scanning time of 6 min and 10 s (Fishman et al., 2015). T1-weighted structural images were obtained using a standard fast spoiled gradient echo T1-weighted sequence with the following parameters: TR/TE=11.08/4.3 ms, TI=1100 ms, 45° flip angle, 128 sagittal slices, matrix size=256×256, FOV=256 mm (Abbott et al., 2016). DTI scans were collected using an echo-planar pulse sequence with the following parameters: TR/TE=8500/84.9 ms, acquisition matrix=128×128, FOV=240 mm, acquisition voxel size=1.88×1.88×2 mm³, 61 non-collinear directions at $b=1000$ s/mm², and 1 at $b=0$ s/mm² (Fishman et al., 2015).

Image preprocessing

T1-weighted imaging

To obtain voxel-wise gray matter volumes of each subject, the T1-weighted images were preprocessed using the voxel-based morphometry (VBM) analysis implemented in Statistical Parametric Mapping 12 (SPM12; Wellcome Department of Cognitive Neurology, University of London) and Computation Anatomy Toolbox with default parameters (CAT 12; Christian Gaser; Department of Psychiatry, University of Jena). All images were first corrected for magnetic field inhomogeneities, then segmented into gray matter (GM), white matter (WM), and cerebrospinal fluid (CSF) (Ashburner & Friston, 2005). The segmentation process was further enhanced by controlling for partial volume effects using a hidden Markov Random Field model (Tohka et al., 2004). All segmented images were spatially normalized using the DARTEL algorithm (Ashburner, 2007). Furthermore, the resulting GM segments were smoothed with a Gaussian kernel of 8 mm (full width at height maximum, FWHM). Finally, total intracranial volume was calculated as the sum of GM, WM, and CSF volumes, and further used as a covariate for the following analyses.

Diffusion tensor imaging

DTI data preprocessing was conducted with a similar procedure to previous work (Bonifazi et al., 2018; He et al.,

2020), where FSL (FMRIB Software Library v5.0.9, <http://www.fmrib.ox.ac.uk/fsl>) and the diffusion toolkit were adopted. First, an eddy current correction was employed to correct the artifacts introduced by head motion or variation in the direction of the gradient fields of the MR scanner (Yamada et al., 2014). Subsequently, the diffusion tensor models were built using the linear least-squares fitting technique at each voxel in Diffusion Toolkit (Wang et al., 2007). For each participant, whole-brain fiber tracking was implemented in native space by using the Fiber Assignment by Continuous Tracking algorithm. Path tracing termination criteria included fractional anisotropy (FA) values less than 0.2 or angular threshold larger than 60°.

Functional imaging

Resting-state functional data were preprocessed using the advanced edition of Data Processing Assistant for Resting-State fMRI (DPARSF A v6.1, <http://rfmri.org/DPARSF>) (Yan et al., 2016). Image preprocessing steps included discarding the first ten volumes, slice-timing correction, spatial realignment (subjects with translational or rotational head motion larger than 3 mm or 3° were excluded), normalization to the Montreal Neurological Institute (MNI) stereotaxic space and then resampling to $3 \times 3 \times 3$ mm³, nuisance covariates regression (Friston 24 motion parameters, the signals from white matter and cerebrospinal fluid), spatial smoothing with a 6 mm full-width at half-maximum Gaussian kernel, the linear detrending and band-pass filtering (0.01–0.08 Hz), and data scrubbing by cubic spline interpolation to fit the motion “spikes” (volumes with frame-wise displacement > 0.5 mm together with the preceding volume and the two succeeding volumes, a conservative strategy ensuring the maximum sample size while accounting for the effects of head motion on our findings) (Power et al., 2012).

Network construction

Morphometry similarity networks (MSNs)

MSNs were constructed by using the GM volume image for each subject. Herein, network nodes were quantified by the 90 (45 for each hemisphere) cortical and subcortical regions of interest (ROIs) from the Automated Anatomical Labeling atlas (AAL) (Tzourio-Mazoyer et al., 2002), and network edges were defined by the symmetric KL divergence-based similarity (KLS) (Wang et al., 2016). For each subject, the GM volume values of all voxels in each ROI were extracted to estimate their probability density function based on the kernel density estimation. Then, the probability distribution function (PDF) was computed to obtain the probability

density function. Subsequently, the KL divergence between any pair of ROIs was defined as:

$$D_{KL}(P, Q) = \sum_{i=1}^n \left(P(i) \log \frac{P(i)}{Q(i)} + Q(i) \log \frac{Q(i)}{P(i)} \right) \quad (1)$$

Where n is the total number of sample points ($n=2^7$ was utilized in the current study, as the same in (Wang et al., 2016)). P and Q were two PDFs. Finally, the KLS was calculated as:

$$KLS(P, Q) = e^{-D_{KL}(P, Q)} \quad (2)$$

The value of KLS ranges from 0 to 1, where 1 represents the identical distributions between the GM P and Q density distributions, and 0 represents the maximum separability.

Structural connectivity networks (SCNs)

The SCN was constructed by using the FA map of each subject. The nodes of SCN were determined by the defined ROIs in the native diffusion space. Accordingly, diffusion imaging of each subject was first coregistered into the corresponding non-diffusion-weighted ($b=0$) images in the native diffusion space through a linear transformation. The coregistered structural images were then mapped to the same stereotactic space as the customized template by using an affine transformation with 12 degrees of freedom accompanied by a series of nonlinear warps. Afterwards, the AAL template was registered into the individual DTI space of each subject through inverse transformation, these 90 ROIs served as the nodes of SCN of each subject. In the native diffusion space, the edge of SCN was defined as the mean FA values of fibers along all fibers connecting the two nodes. SCN is a symmetric matrix, where the connectivity from node i to node j is equal to that from j to i .

Functional connectivity networks (FCNs)

For the preprocessing image of each subject, the AAL was utilized to divide the brain into 90 ROIs. The time series of each ROI was generated by averaging the time series of all voxels within it, and the Pearson correlation coefficient between any pair of ROIs was computed as the edge of FCN. The correlation coefficients were normalized by the Fisher’s transformation:

$$Z = \frac{1}{2} \sqrt{n-3} \times \ln \left(\frac{1+r}{1-r} \right) \quad (3)$$

Where n denotes the number of time points and r denotes the correlation coefficients between ROIs.

Classification analysis

Feature selection

In the current study, the NYU, which is considered as an independent dataset, was employed in the feature selection. From the original connectivity matrix from fMRI, DTI, and sMRI for each participant, three different classes of features were respectively generated: functional connectivity (FC) from FCN, structural connectivity (SC) from SCN, and morphological connectivity (MC) from MSN. Given that 90 ROIs were applied in these networks, each participant had 12,015 features ($[90 \times (90 - 1) / 2] \times 3$ [MC, SC, and FC]). After the combination of the three classes of features and normalization, the feature matrix had $N \times 12,015$ dimensions (N number of individuals times 12015 features). To avoid redundant features and reduce the matrix dimension, recursive feature elimination with cross-validation (RFECV) was conducted (Guyon et al., 2002). In addition, all features were controlled for the nuisance covariates including the age, gender, full-scale IQ (FIQ), and mean frame-wise displacement (meanFD).

Support vector machine classifier

In the current study, a support vector machine (SVM) model was adopted for classification in the SDSU dataset. SVM performs well despite that the size of the sample is small while the total number of features is large. SVM classification is a supervised learning method and commonly used in prior studies. To estimate the robustness of classification from the SVM models, the leave-one-out cross-validation (LOOCV) strategy was performed. In each LOOCV trail, the SVM model was built based on $n-1$ training samples and then predicted a new label (i.e., 1 represents ASD and -1 represents TDC) in the remaining one. This process was repeated until all participants had their new label. To obtain summary classification performance, the statistics including accuracy, sensitivity, specificity, and receiver operating characteristic (ROC) were calculated, and then the area under the curve was estimated to illustrate the overall performance of the method. That is,

$$\text{Sensitivity} = \frac{TP}{TP + FN} \quad (4)$$

$$\text{Specificity} = \frac{TN}{TN + FP} \quad (5)$$

$$\text{Accuracy} = \frac{(TP + TN)}{TP + TN + FP + FN} \quad (6)$$

Where TP, FP, TN, and FN denote the number of true positives, false positives, true negatives, and false negatives, respectively (Son et al., 2010).

The statistical significance of classification accuracy was examined using permutation tests. In each permutation, the group labels were shuffled and the same classification procedure was repeated to acquire an Acc_{perm} value. This permutation process was repeated 5000 times, and the final P value was obtained by calculating the proportion of the number of times that Acc_{perm} is greater or equal to the actual Acc -value in total permutation times (Mu et al., 2020). Classification model with single modes (including fMRI, DTI, or sMRI) and different modal combinations (including fMRI+DTI, fMRI+sMRI, DTI+sMRI, and fMRI+DTI+sMRI) (Fig. 1) (Zhao et al., 2020).

Relationship with autistic symptoms

A linear support vector regression (SVR) was conducted to evaluate autistic patients' symptom severity scores based on the top 10% connections after ranking the weight in SVM. Leave-one-out validation (LOOCV) strategy was employed to assess the performance of the evaluation. For LOOCV, the evaluated values from "left-out" participants were generated by taking the training data from all other participants and repeating this process until all participants had an evaluated value. The correlation coefficient was computed between the actual symptom scores and their corresponding evaluated score. A permutation test with 10,000 times was employed to consider the statistical significance of these correlation coefficients.

Results

Demographic variables and clinical measures

47 TDC and 50 ASD individuals were selected from ABIDE II in this manuscript. The two-sample t-test showed that the distribution of age, gender, MeanFD, and the proportion of scrubbed time points (number of "bad" time points/total time points, PST) in ASD were not significantly different from that of TDC, but the FIQ was significantly lower in the ASD group than that in the TDC group. Detailed information of enrolled subjects is shown in Table 1.

Classification accuracy

In this study, we found a classification accuracy of 82.69% (85.71% sensitivity, 79.19% for specificity, permutation test $p < 0.001$, 5000 loops) after combining the network features of fMRI, sMRI and DTI modalities (Fig. 2; Table 2).

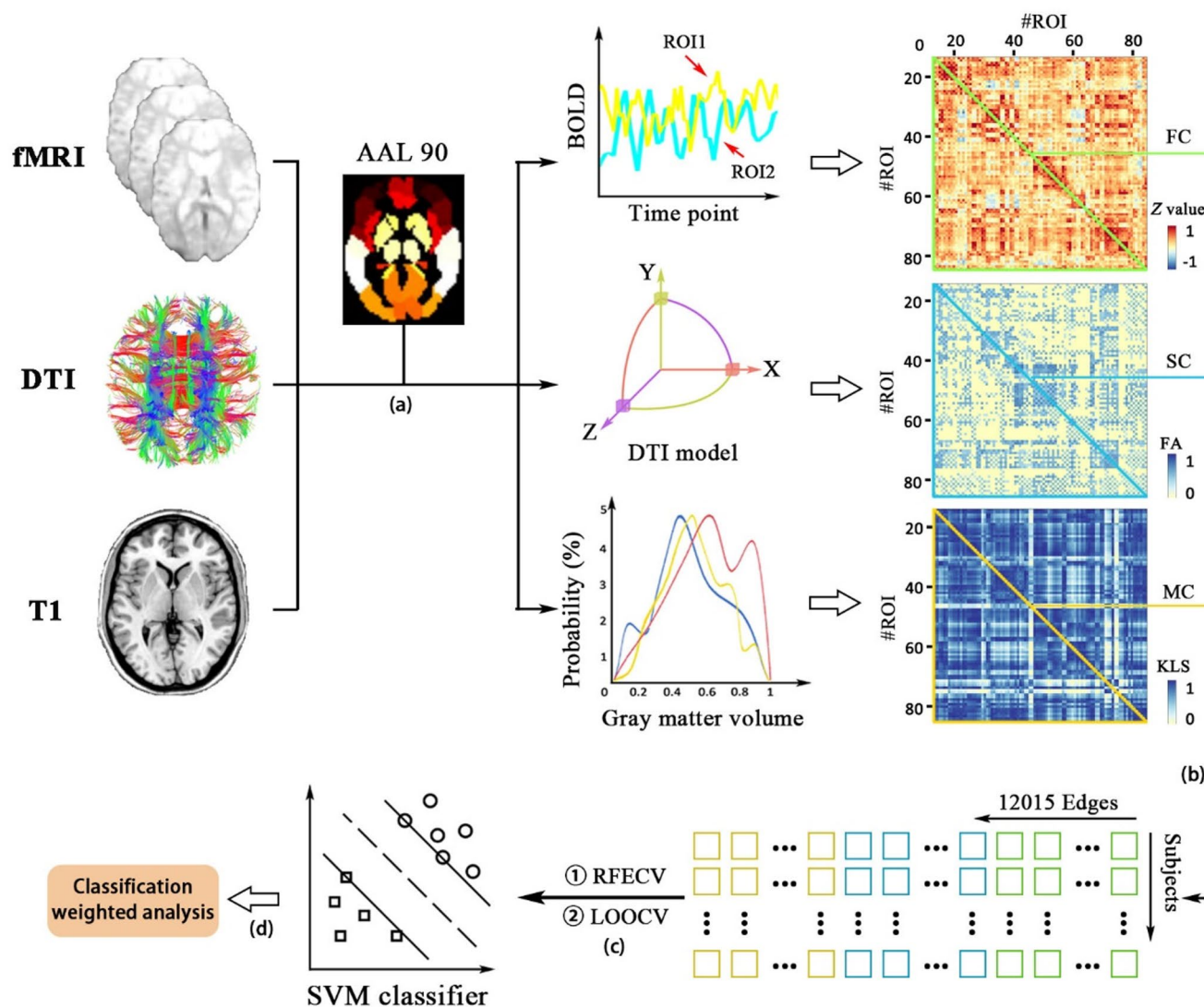


Fig. 1 Methodological sketch. **a**) Network construction based on AAL 90 ROIs. Individual functional (FC, fMRI), structural (SC, DTI), and morphological (MC, T1) connectivity matrices were built for each participant after image preprocessing. **b**) Features obtained from MC, SC, and FC were used to perform classification. **c**) Feature selection: removing the redundant features using the RFECV and eliminating the effect of age, gender, FIQ, and meanFD. **d**) Classification model construction: The SVM model and LOOCV were applied in classifying the

ASD and TDC labels. ASD, autism spectrum disorder; TDC, typically developing control; FIQ, full-scale IQ; Mean FD, mean frame-wise displacement; KLS, KL divergence-based similarity; SVM, support vector machine; LOOCV, leave-one-out cross-validation; RFECV, recursive feature elimination with cross-validation; MC, morphological connectivity; SC, structural connectivity; FC, functional connectivity; AAL, Automated Anatomical Labeling atlas

The classification accuracy achieved by combining all three modalities (including fMRI+DTI+sMRI) was significantly higher compared to that using any combination of two modalities (including fMRI+DTI, fMRI+sMRI, or DTI+sMRI). Moreover, the accuracy obtained using two modalities (including fMRI+DTI, fMRI+sMRI, or DTI+sMRI) was significantly greater than that achieved using a single modality (i.e., fMRI, sMRI or DTI, $P < 0.05$ for all comparisons, permutation test). These results suggest that each modality plays a crucial synergistic role in

supporting the classification performance. Please refer to Fig. 2; Table 2 for further details.

Feature selection in high-classification performance

485 connections were selected using the RFECV technique based on the NYU dataset (Fig. S1) and then were used in the SVM for ASD vs. DTC classification of participants from the SDSU dataset. After weight ranking in the optimal SVM, we identified the top 10% connections with the highest ranks, resulting in a total of 49 connections. Among

Table 1 Participant demographics

Variables	SDSU			NYU		
	ASD (<i>n</i> =28)	TDC (<i>n</i> =24)	<i>P</i> -value	ASD (<i>n</i> =22)	TDC (<i>n</i> =23)	<i>P</i> -value
Age	13.5±3.07	13.4±3.02	0.87 ^a	8.4±2.98	9.2±1.91	0.28 ^a
Gender (M/F)	22/6	22/2	0.19 ^b	21/1	23/0	0.30 ^b
FIQ	99.4±14.7	102.8±11.9	0.36 ^a	103.3±18.2	116.0±15	<i>P</i> =0.01 ^a
MeanFD	0.16±0.09	0.16±0.12	0.95 ^a	0.22±0.11	0.20±0.13	0.58 ^a
PST	0.09±0.11	0.10±0.19	0.68 ^a	0.17±0.16	0.15±0.18	0.67 ^a
ADI-R						
Social interaction	18.93±4.18	--	--	17.5±7.31	--	--
Communication	13.6±4.6	--	--	15.68±5.11	--	--
RRB	5.75±2.38	--	--	5.09±3.22	--	--

ASD, autism spectrum disorder; TDC, typically developing control; FIQ, full-scale IQ; Mean FD, mean framewise displacement; PST, proportion of scrubbed time-points (number of “bad” time points/total time points); Mean±Standard deviation; M, male; F, female; ADI-R, Autism Diagnostic Interview-Revised; RRB, restricted, repetitive, and stereotyped behaviors. “Bad” time points denote time points with frame-wise displacement>0.5 mm, including the preceding time point and the two succeeding time points

^a The *P* value was obtained by a two-sample *t*-test, two-tailed

^b The *P* value was obtained by the Kruskal–Wallis test

these connections, 24 were derived from the SCN, 21 from the FCN, and 4 from the MSN. Specifically, the structural connections primarily involved the temporal, parietal, and occipital lobes. The functional connections were predominantly observed in the prefrontal and occipital lobes, while the morphological connections primarily involved the temporal lobe (Fig. 3).

Classification multimodal connectivity features (including fMRI + DTI + sMRI) predict symptom severity in ASD

After performing an SVR method, the top 10% connections after weight-ranking were found to predict social interaction deficits ($r=0.66$, permutation test $p<0.001$, 10000 times, Fig. 4)(DiCiccio & Romano, 2017).

Reproducibility and replicability analysis

To investigate the robustness of our findings, we made use of the SDSU dataset for feature selection (see Figure S2), while the NYU dataset was employed for the SVM analysis. Remarkably, when combining all three modalities (including fMRI+DTI+sMRI) for classification, we achieved an accuracy of 80%, along with a sensitivity of 81.82% and specificity of 78.26% (permutation test, $p<0.001$, 5000 iterations, table S1 and Figure S3).

Discussion

The current study makes use of brain neuroimaging data from fMRI, sMRI and DTI modalities to construct FCN, MSN, and SCN for each participant, to identify biomarkers

of brain connectivity in individuals with ASD. The results can be summarized as follows: (1) A discriminant accuracy of 82.69% for ASD classification was accomplished after integrating the connectivity patterns from fMRI, sMRI and DTI modalities, and this accuracy was higher than that using one modality (i.e., fMRI, sMRI, or DTI) or two-modalities (including fMRI+DTI, fMRI+sMRI, or DTI+sMRI) classes; (2) the relatively high classification accuracy was contributed by those connectivity features mainly involving in the temporal, occipital and parietal networks from the DTI modality, prefrontal and parietal networks from the fMRI modality, and temporal networks from the sMRI modality; (3) the connectivity pattern of the fMRI, sMRI and DTI modalities predicted the severity of social interaction deficits in individuals with ASD. The results highlight the critical role of a multimodal connectivity biomarker (i.e., connectivity patterns derived from the fMRI, sMRI and DTI modalities) in the pathophysiology of ASD.

In the current study, the individual MSN was constructed based on KL divergence to measure similarities in the distribution of gray matter volume. Such methods were first utilized by Kong et al. (Kong et al., 2014) and further developed by Wang et al. (Wang et al., 2016). These authors discovered that MSN analysis at the individual level is a significant and reliable method for characterizing human brain organization and structure. Our results indicate that this method attained an accuracy of 73.08%, whereby the connections majorly involved were part of the social brain network including the amygdala, fusiform, thalamus, heschl gyrus, caudate, and middle frontal gyrus. Previous studies have reported that the social brain network is responsible for processing social information and is impaired in autistic patients (Sato et al., 2012, 2017). Our findings further support the relevance of this MSN for the diagnosis of ASD.

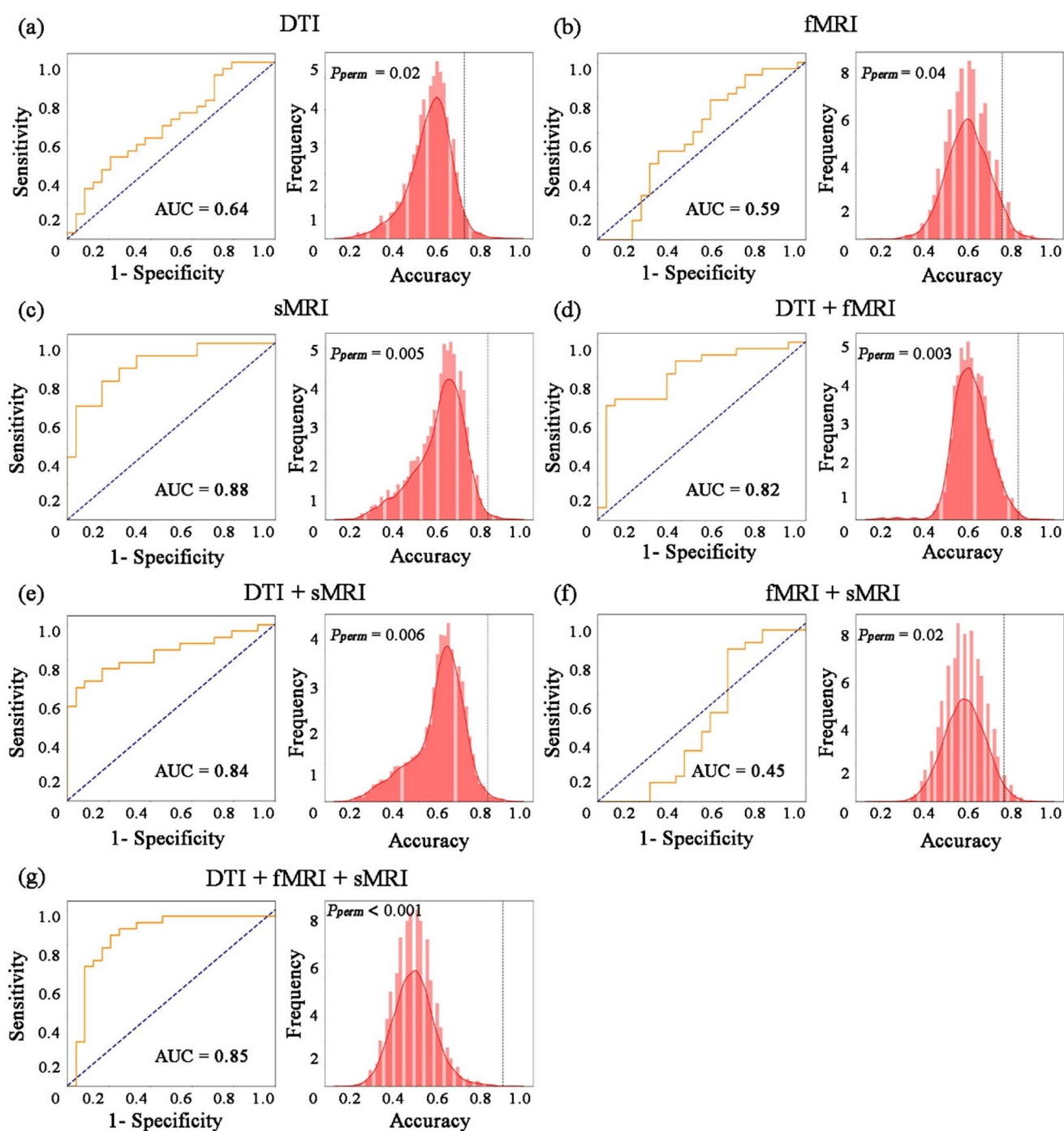


Fig. 2 Classification performance using different modality features in the SDSU dataset. **(a)** Performance of classifying ASD and TDC labels based on structural connectivity features (i.e., DTI). The left panel shows the ROC curve of the classifier and the right panel shows the frequency distribution of accuracy using 5000 permutation tests. The vertical dashed line on the x-axis is the actual classification accu-

racy. **(b-g)** Similar to **(a)** but for functional connectivity features (i.e., fMRI), morphological connectivity features (i.e., sMRI), DTI+fMRI, DTI+sMRI, fMRI+sMRI, and DTI+fMRI+sMRI, respectively. ROC, receiver operating characteristic. ASD, autism spectrum disorder; TDC, typically developing control

The classification accuracy of the SCNs reached 67.31%. In addition, these DTI connections using the SVM classifier were primarily distributed in temporal, parietal, and occipital lobes. Diffusion tensor imaging (DTI) studies of white

matter integrity revealed similar atypical connectivity patterns in individuals with developing autistic brains (Spurgin, 2007). A recent theory that attempts to reconcile the conflicting results in the literature suggests that hyperconnectivity

Table 2 Results of the ASD classification using different modality features in the SDSU dataset

	Accuracy (%)	Sensitivity (%)	Specificity (%)
DTI	67.31	67.86	66.67
fMRI	61.54	82.13	37.5
sMRI	73.08	64.29	83.33
DTI+fMRI	73.07	67.86	79.17
DTI+sMRI	75	78.57	70.83
fMRI+sMRI	63.46	85.71	37.5
DTI+fMRI+sMRI	82.69	85.71	79.17

of brain networks may be more characteristic in young children with ASD, whereas hypoconnectivity is more prevalent in adolescents and adults with the disorder compared with individuals with typical development (TD) (He et al., 2020; Nomi & Uddin, 2015). Furthermore, two pathways of the temporal-occipital cortex and temporal-parietal junction in ASD were investigated to play an important role in social cognition. Ameis et al. have investigated that the temporal-occipital circuit was involved in social-emotional processing in children with ASD (Ameis et al., 2011) and David et al. have reported that the disruption in the temporal-parietal junction was positively correlated with social motion perception in ASD (David et al., 2014). Here, following previous works (Di Martino et al., 2014; Supekar et al., 2013), SCN patterns related to abnormal social behavior at the network level may be regarded as a significant marker for the diagnosis of ASD.

FCNs have been constructed using resting-state fMRI, in which brain connections of the prefrontal and occipital lobes have been mainly used as features for classification, yielding a diagnostic accuracy of approximately 61.54%. Recently, fMRI studies have reported connectivity of the frontoparietal network, a circuitry central to the completion of social coordination (Dumas et al., 2020), shown relevant for autism symptomatology (Lin et al., 2019). In line with previous studies, we found that the functional connections more relevant for classification (with higher weights in the performed classifier) were related to the prefrontal and parietal networks. Although the connections were not coincident with those detected by the DTI modalities, the performance of the FCN was lower than the one achieved by the structural network, in agreement with previous work (Roland et al., 2017). Functional connections can also be observed between regions with few structural connections or no connections, which suggests the indirect connections mediating functional association through third-common neighbors during brain development (Honey et al., 2009). Thus, the information acquired from FCN cannot be ignored in studying the development of the autistic brain.

After combining the network connections from the fMRI, sMRI and DTI modalities, we have built connectivity features for a diagnostic accuracy higher than that obtained using any single modality (Fig. 2 and Figure S3). Brain networks constructed via different modalities may reflect different aspects of brain architecture. Indeed, some authors showed specifically that MSNs using cortex thickness correlations differed significantly from white matter networks constructed using DTI (Gong et al., 2012). Moreover, although some previous studies have shown that a combination of different brain network modalities did not increase classification performance (Reid et al., 2016), our study shows a high synergistic power to predict ASD by the combination of the top 10% connections after weight-ranking from fMRI, sMRI, and DTI modalities and further demonstrated that these connections were closely related to social-interaction symptoms of ASD. Such differences may be related to the influence of genetic risk factors on different brain tissues in different manners or at different stages in autistic brain development (Shi et al., 2012) and suggest that the combination of multimodal features provided complementary information carried by different biomarkers. In addition to achieving excellent performance in ASD classification, the integrated set of connections from the fMRI, sMRI and DTI modalities also showed a good performance in predicting the severity of the social interaction deficits. This finding may indicate that these connections might be relevant for explaining abnormal social behavior in ASD and further reflect the severity of ASD. This brain-behavior association also underscores the potential importance of brain networks from the fMRI, sMRI and DTI modalities to distinguish individuals with ASD and may contribute to developing an objective biomarker of ASD.

Limitations

Several limitations of the current study should be noted. First, the sample size was relatively modest owing to the age range (5–18 years) and the brain connectivity network generated using fMRI, sMRI, and DTI in ASD. Larger sample sizes are required to replicate and confirm our results. Second, we employed simple combination methods and ignored the relationships between the different modalities. This is beyond the scope of the present work and should be addressed in future studies. Third, the morphological connectivity in the current study was generated from the probability distributions of morphological variables acquired from structural neuroimaging. Such distributions require an accurate assessment. In this study, ROIs have been quantified by the AAL atlas widely used for brain network constructions (Gong et al., 2009; Zhang et al., 2011). This atlas displayed sufficiently large observations for each brain area

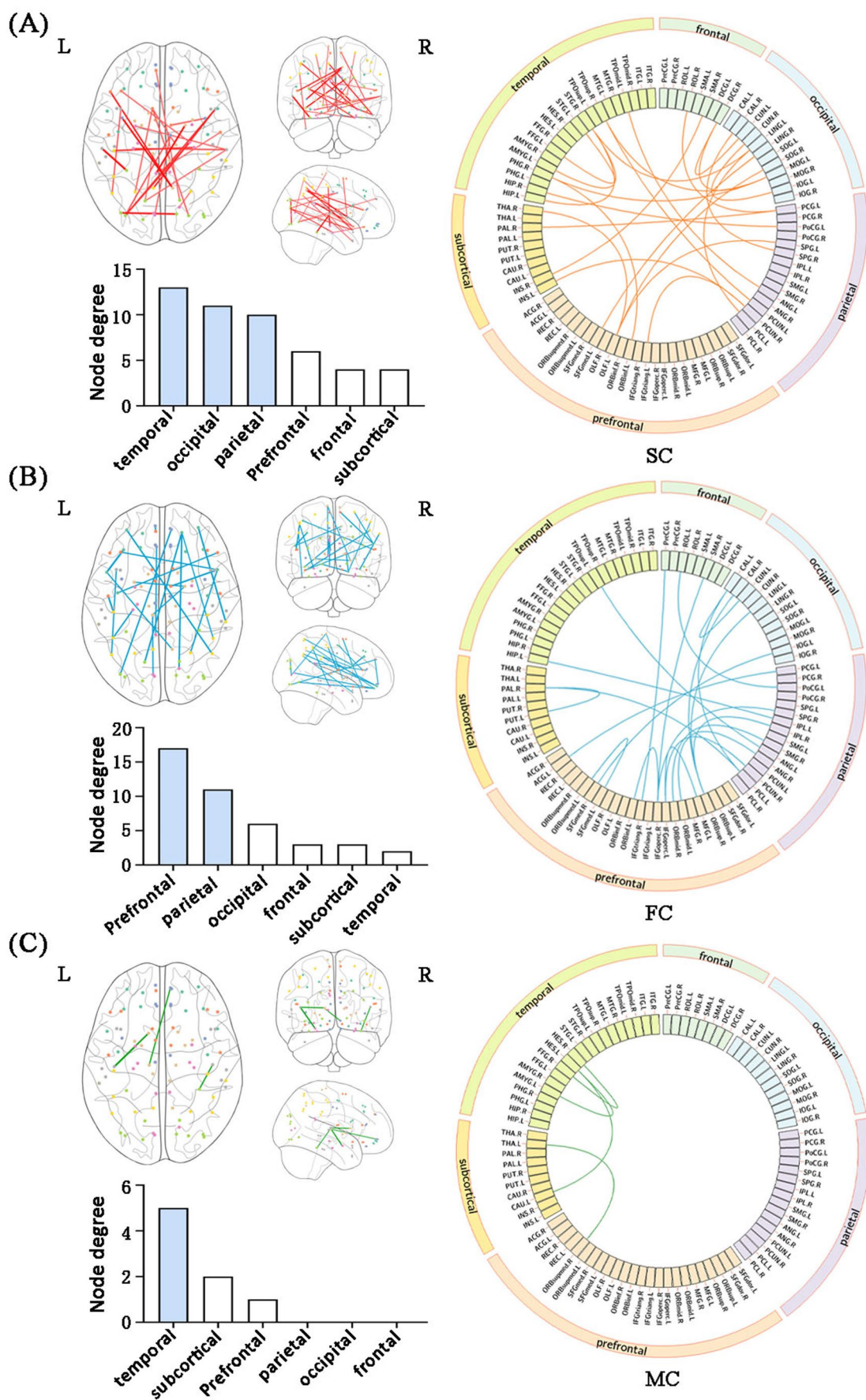


Fig. 3 Distribution of the top 10% highest-weight connections in the optimal SVM solution. (A) 24 structural connections represented by red lines in the glass brains and the wheel-graph connectivity plot. The different ROIs were grouped in six different networks, depicted with a different color in the wheel brain plots. For each region, the total node degree is represented in the histogram. Blue-colored rectangles represent values of total node degrees larger than 50% of the same value but across all different networks. (B-C) Similar to (A) but for the 21 functional connections and 4 morphological connections. MC, morphological connectivity; SC, structural connectivity; FC, functional connectivity; AAL, anatomical automatic labeling atlas. SVM, support vector machine; ROI, region of interest; L, left; R, right

(larger than 120) and enabled the accurate evaluation of regional morphological distributions. However, previous fMRI or diffusion MRI studies have reported that structural and functional templates do not correspond to the same physical and physiological mechanisms (Diez et al., 2015). A comparison of the current results with those based on different templates is vital to provide comprehensive insights into the effect of different brain parcellation schemes on the coherent organization of brain networks within the fMRI, sMRI and DTI modalities. Fourth, although a reliable ROI-wise morphological connectivity has been generated by using the KLS technique (Kong et al., 2015; Wang et al., 2016; Zhao et al., 2020), further research is still required to identify the extent of how morphological connectivity in the brain can reflect its structural or functional connectivity. Finally, to our knowledge, the prevalence of ASD is higher among boys, and it is hard to recruit female subjects with ASD. Only including male subjects limits our ability to investigate the potential impact of gender factors on our findings. In future research, larger datasets including female subjects are needed.

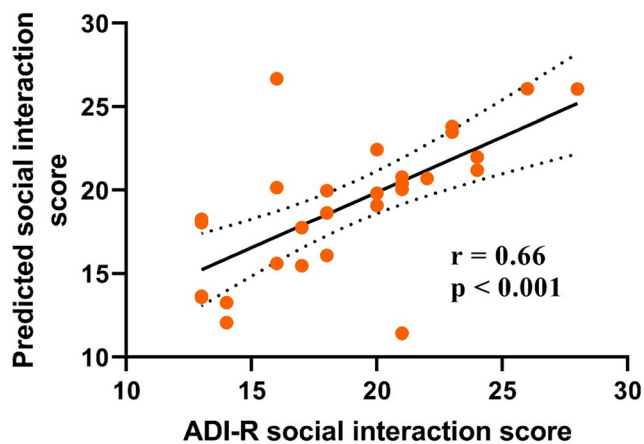


Fig. 4 Correlation between predicted and observed values in the ADI-R social interaction sub-score in autistic participants. Solid and dashed lines denote respectively the best-fitted line and 95% confidence interval of Pearson's correlation analysis. ASD, autism spectrum disorder, ADI-R, Autism Diagnostic Interview-Revised

Conclusion

We found relative accuracy in classifying ASD and TDC using connectivity features combining three different brain imaging modalities (i.e., functional, structural, and morphological connectivities), which was superior to using any single modality (i.e., fMRI, sMRI or DTI) or combinations of two modalities (including fMRI+DTI, fMRI+sMRI, or DTI+sMRI). Furthermore, we also found a significant association of the connectivity features from fMRI, sMRI and DTI modalities with abnormal social behavior in ASD. These results suggest that the combination of multiple modalities could be effectively utilized to obtain complementary information regarding brain connectivity networks and may be helpful to offer clinically relevant biomarkers of neurological syndromes in ASD.

Supplementary Information The online version contains supplementary material available at <https://doi.org/10.1007/s11682-025-01026-5>.

Acknowledgements We are grateful to all the participants and their guardians in this study.

Author contributions Changchun He, Xujun Duan, Huafu Chen conceptualized and designed the study. Changchun He, Heng Chen, Xiaolong Shan, and Maoyang Zou contributed to the analysis and interpretation of data. Changchun He, Xujun Duan, and Jesus M. Cortes drafted the manuscript and prepared Figs. 1, 2, 3 and 4; Table 1, and 2. Changchun He, Xujun Duan, Jesus M. Cortes, Xianmin Wang, Yi Ding, Heng Chen revised the manuscript critically for important intellectual content.

Funding This research was supported by the Fundamental Research Fund for the Chengdu University of Information Technology (No. KYTZ2023043), Higher Education Teaching Research and Reform Fund (No. JYJG2024165), One-time funding for the FT-042 Postdoctoral Research Station (No. XM25-10691), Higher Education Teaching Research and Reform Fund (No. JYJG2024165) and the Natural Science Foundation of Sichuan Province (No. 2023NSFSC0482).

Data availability All data in the current study were available from the public dataset (Autism Brain Imaging Data Exchange II [ABIDE II], https://fcon_1000.projects.nitrc.org/indi/abide/)

Code availability Not applicable.

Declarations

Ethics approval This study was approved by the institutional review boards of the New York University and the San Diego State University Institutional Review Boards.

Consent to participate Not applicable.

Consent for publication Not applicable.

Competing interests The authors declare no competing interests.

References

- Abbott, A. E., Nair, A., Keown, C. L., Datko, M., Jahedi, A., Fishman, I., & Muller, R. (2016). Patterns of atypical functional connectivity and behavioral links in autism differ between default, salience, and executive networks. *Cerebral Cortex*, *26*(10), 4034–4045.
- Alexander, A. L., Lee, J. E., Lazar, M., Boudos, R., DuBray, M. B., Oakes, T. R., & McMahon, W. M. (2007). Diffusion tensor imaging of the corpus callosum in autism. *Neuroimage*, *34*(1), 61–73.
- Ameis, S. H., Fan, J., Rockel, C., Voineskos, A. N., Lobaugh, N. J., Soorya, L., & Anagnostou, E. (2011). Impaired structural connectivity of socio-emotional circuits in autism spectrum disorders: A diffusion tensor imaging study. *Plos One*, *6*(11), e28044.
- Ashburner, J. (2007). A fast diffeomorphic image registration algorithm. *Neuroimage*, *38*(1), 95–113.
- Ashburner, J., & Friston, K. J. (2005). Unified segmentation. *Neuroimage*, *26*(3), 839–851.
- Association American Psychiatric (2013). Diagnostic and statistical manual of mental disorders, 5th edition: DSM-5. *Psychosomatics*, *29*(1), 133–134.
- Baron-Cohen, S., Leslie, A. M., & Frith, U. (1985). Does the autistic child have a theory of Mind?? *Cognition*, *21*(1), 37–46.
- Bashat, D. B., Kronfeld-Duenias, V., Zachor, D. A., Ekstein, P. M., Hendler, T., Tarrasch, R., & Sira, L. B. (2007). Accelerated maturation of white matter in young children with autism: A high B value DWI study. *Neuroimage*, *37*(1), 40–47.
- Bonifazi, P., Erramuzpe, A., Diez, I., Gabilondo, I., Boisgontier, M. P., Pauwels, L., & Cortes, J. M. (2018). Structure–function multi-scale connectomics reveals a major role of the fronto-striato-thalamic circuit in brain aging. *Human Brain Mapping*, *39*(12), 4663–4677.
- Cheng, Y., Chou, K. H., Chen, I. Y., Fan, Y. T., Decety, J., & Lin, C. P. (2010). Atypical development of white matter microstructure in adolescents with autism spectrum disorders. *Neuroimage*, *50*(3), 873–882.
- Cociu, B. A., Das, S., Billeci, L., Jamal, W., Maharatna, K., Calderoni, S., & Muratori, F. (2017). Multimodal functional and structural brain connectivity analysis in autism: A preliminary integrated approach with EEG, fMRI, and DTI. *IEEE Transactions on Cognitive and Developmental Systems*, *10*(2), 213–226.
- Courchesne, E., Carper, R., & Akshoomoff, N. (2003). Evidence of brain overgrowth in the first year of life in autism. *Jama*, *290*(3), 337–344.
- Courchesne, E., Pierce, K., Schumann, C. M., Redcay, E., Buckwalter, J. A., Kennedy, D. P., & Morgan, J. (2007). Mapping early brain development in autism. *Neuron*, *56*(2), 399–413.
- David, N., Schultz, J., Milne, E., Schunke, O., Schöttle, D., Münchau, A., & Engel, A. K. (2014). Right temporoparietal Gray matter predicts accuracy of social perception in the autism spectrum. *Journal of Autism and Developmental Disorders*, *44*, 1433–1446.
- Di Martino, A., Yan, C. G., Li, Q., Denio, E., Castellanos, F. X., Alaerts, K., & Dapretto, M. (2014). The autism brain imaging data exchange: Towards a large-scale evaluation of the intrinsic brain architecture in autism. *Molecular Psychiatry*, *19*(6), 659–667.
- Di Martino, A., O’connor, D., Chen, B., Alaerts, K., Anderson, J. S., Assaf, M., & Bernaerts, S. (2017). Enhancing studies of the connectome in autism using the autism brain imaging data exchange II. *Scientific Data*, *4*(1), 1–15.
- DiCiccio, C. J., & Romano, J. P. (2017). Robust permutation tests for correlation and regression coefficients. *Journal of the American Statistical Association*, *112*(519), 1211–1220.
- Diez, I., Bonifazi, P., Escudero, I., Mateos, B., Muñoz, M. A., Stramaglia, S., & Cortes, J. M. (2015). A novel brain partition highlights the modular skeleton shared by structure and function. *Scientific Reports*, *5*(1), 10532.
- Dumas, G., Moreau, Q., Tognoli, E., & Kelso, J. S. (2020). The human dynamic clamp reveals the fronto-parietal network linking real-time social coordination and cognition. *Cerebral Cortex*, *30*(5), 3271–3285.
- ElNakieb, Y., Ali, M. T., Dekhil, O., Khalefa, M. E., Soliman, A., Shalaby, A., & Elmaghraby, A. (2018). Towards accurate personalized autism diagnosis using different imaging modalities: sMRI, fMRI, and DTI. Paper presented at the 2018 IEEE International Symposium on Signal Processing and Information Technology (ISSPIT).
- Evans, A. C. (2013). Networks of anatomical covariance. *Neuroimage*, *80*, 489–504.
- Fishman, I., Datko, M., Cabrera, Y., Carper, R. A., & Müller, R. A. (2015). Reduced integration and differentiation of the imitation network in autism: A combined functional connectivity magnetic resonance imaging and diffusion-weighted imaging study. *Annals of Neurology*, *78*(6), 958–969.
- Fox, M. D. (2018). Mapping symptoms to brain networks with the human connectome. *New England Journal of Medicine*, *379*(23), 2237–2245.
- Gong, G., He, Y., Concha, L., Lebel, C., Gross, D. W., Evans, A. C., & Beaulieu, C. (2009). Mapping anatomical connectivity patterns of human cerebral cortex using in vivo diffusion tensor imaging tractography. *Cerebral Cortex*, *19*(3), 524–536.
- Gong, G., He, Y., Chen, Z. J., & Evans, A. C. (2012). Convergence and divergence of thickness correlations with diffusion connections across the human cerebral cortex. *Neuroimage*, *59*(2), 1239–1248.
- Guo, X., Chen, H., Long, Z., Duan, X., Zhang, Y., & Chen, H. (2017). Atypical developmental trajectory of local spontaneous brain activity in autism spectrum disorder. *Scientific Reports*, *7*, 1–10.
- Guyon, I., Weston, J., Barnhill, S., & Vapnik, V. (2002). Gene selection for cancer classification using support vector machines. *Machine Learning*, *46*, 389–422.
- He, C., Chen, H., Uddin, L. Q., Erramuzpe, A., Bonifazi, P., Guo, X., & Li, L. (2020). Structure–function connectomics reveals aberrant developmental trajectory occurring at preadolescence in the autistic brain. *Cerebral Cortex*, *30*(9), 5028–5037.
- He, C., Cortes, J. M., Kang, X., Cao, J., Chen, H., Guo, X., & Xiao, J. (2021). Individual-based morphological brain network organization and its association with autistic symptoms in young children with autism spectrum disorder. *Human Brain Mapping*, *42*(10), 3282–3294.
- Hermundstad, A. M., Bassett, D. S., Brown, K. S., Aminoff, E. M., Clewett, D., Freeman, S., & Miller, M. B. (2013). Structural foundations of resting-state and task-based functional connectivity in the human brain. *Proceedings of the National Academy of Sciences*, *110*(15), 6169–6174.
- Honey, C. J., Sporns, O., Cammoun, L., Gigandet, X., Thiran, J. P., Meuli, R., & Hagmann, P. (2009). Predicting human resting-state functional connectivity from structural connectivity. *Proceedings of the National Academy of Sciences*, *106*(6), 2035–2040.
- Jeste, S. S., Frohlich, J., & Loo, S. K. (2015). Electrophysiological biomarkers of diagnosis and outcome in neurodevelopmental disorders. *Current Opinion in Neurology*, *28*(2), 110.
- Keller, T. A., Kana, R. K., & Just, M. A. (2007). A developmental study of the structural integrity of white matter in autism. *Neuroreport*, *18*(1), 23–27.
- Kong, X., Wang, X., Huang, L., Pu, Y., Yang, Z., Dang, X., & Liu, J. (2014). Measuring individual morphological relationship of cortical regions. *Journal of Neuroscience Methods*, *237*, 103–107.
- Kong, X., Liu, Z., Huang, L., Wang, X., Yang, Z., Zhou, G., & Liu, J. (2015). Mapping individual brain networks using statistical

- similarity in regional morphology from MRI. *Plos One*, 10(11), e0141840.
- Koyama, M. S., Martino, A. D., Kelly, C., Jutagir, D. R., Sunshine, J., Schwartz, S. J., & Milham, M. P. (2013). Cortical signatures of dyslexia And remediation: An intrinsic functional connectivity approach. *Plos One*, 8(2), e55454.
- Lin, H. Y., Perry, A., Cocchi, L., Roberts, J. A., Tseng, W. Y. I., Breakspear, M., & Gau, S. S. F. (2019). Development of frontoparietal connectivity predicts longitudinal symptom changes in young people with autism spectrum disorder. *Translational Psychiatry*, 9(1), 86.
- Mu, J., Chen, T., Quan, S., Wang, C., Zhao, L., & Liu, J. (2020). Neuroimaging features of whole-brain functional connectivity predict attack frequency of migraine. *Human Brain Mapping*, 41(4), 984–993.
- Nomi, J. S., & Uddin, L. Q. (2015). Developmental changes in large-scale network connectivity in autism. *NeuroImage: Clinical*, 7, 732–741.
- Power, J. D., Barnes, K. A., Snyder, A. Z., Schlaggar, B. L., & Petersen, S. E. (2012). Spurious but systematic correlations in functional connectivity MRI networks arise from subject motion. *Neuroimage*, 59(3), 2142–2154.
- Rakić, M., Cabezas, M., Kushibar, K., Oliver, A., & Lladó, X. (2020). Improving the detection of autism spectrum disorder by combining structural and functional MRI information. *NeuroImage: Clinical*, 25, 102181.
- Rasero, J., Jimenez-Marin, A., Diez, I., Toro, R., Hasan, M. T., & Cortes, J. M. (2023). The Neurogenetics of Functional Connectivity Alterations in Autism: Insights From Subtyping in 657 Individuals. *Biological Psychiatry*.
- Reid, A. T., Lewis, J., Bezgin, G., Khundrakpam, B., Eickhoff, S. B., McIntosh, A. R., & Evans, A. C. (2016). A cross-modal, cross-species comparison of connectivity measures in the primate brain. *Neuroimage*, 125, 311–331.
- Roland, J. L., Snyder, A. Z., Hacker, C. D., Mitra, A., Shimony, J. S., Limbrick, D. D., & Leuthardt, E. C. (2017). On the role of the corpus callosum in interhemispheric functional connectivity in humans. *Proceedings of the National Academy of Sciences*, 114(50), 13278–13283.
- Sato, W., Toichi, M., Uono, S., & Kochiyama, T. (2012). Impaired social brain network for processing dynamic facial expressions in autism spectrum disorders. *Bmc Neuroscience*, 13, 1–17.
- Sato, W., Kochiyama, T., Uono, S., Yoshimura, S., Kubota, Y., Sawada, R., & Toichi, M. (2017). Reduced Gray matter volume in the social brain network in adults with autism spectrum disorder. *Frontiers in Human Neuroscience*, 11, 395.
- Shi, F., Yap, P. T., Gao, W., Lin, W., Gilmore, J. H., & Shen, D. (2012). Altered structural connectivity in neonates at genetic risk for schizophrenia: A combined study using morphological and white matter networks. *Neuroimage*, 62(3), 1622–1633.
- Son, Y. J., Kim, H. G., Kim, E. H., Choi, S., & Lee, S. K. (2010). Application of support vector machine for prediction of medication adherence in heart failure patients. *Healthcare Informatics Research*, 16(4), 253–259.
- Spisak, T., Jakab, A., Kis, S. A., Opposits, G., Aranyi, C., Berenyi, E., & Emri, M. (2014). Voxel-wise motion artifacts in population-level whole-brain connectivity analysis of resting-state FMRI. *Plos One*, 9(9), e104947.
- Spurgin, A. A. (2007). Diffusion tensor imaging in children and adolescents: A technology review. *Stanford J Neurosci*, 1(1), 15–17.
- Supekar, K., Uddin, L. Q., Khouzam, A., Phillips, J., Gaillard, W. D., Kenworthy, L. E., & Menon, V. (2013). Brain hyperconnectivity in children with autism and its links to social deficits. *Cell Reports*, 5(3), 738–747.
- Tohka, J., Zijdenbos, A., & Evans, A. (2004). Fast and robust parameter Estimation for statistical partial volume models in brain MRI. *Neuroimage*, 23(1), 84–97.
- Tzourio-Mazoyer, N., Landeau, B., Papathanassiou, D., Crivello, F., Etard, O., Delcroix, N., & Joliot, M. (2002). Automated anatomical labeling of activations in SPM using a macroscopic anatomical parcellation of the MNI MRI single-subject brain. *Neuroimage*, 15(1), 273–289.
- Uddin, L. Q., Supekar, K., & Menon, V. (2013). Reconceptualizing functional brain connectivity in autism from a developmental perspective. *Frontiers in Human Neuroscience*, 7, 458.
- Wang, R., Benner, T., Sorensen, A. G., & Wedeen, V. J. (2007). *Diffusion toolkit: a software package for diffusion imaging data processing and tractography*. Paper presented at the Proc Intl Soc Mag Reson Med.
- Wang, H., Jin, X., Zhang, Y., & Wang, J. (2016). Single-subject morphological brain networks: Connectivity mapping, topological characterization and test–retest reliability. *Brain and Behavior*, 6(4), e00448.
- Yamada, H., Abe, O., Shizukuishi, T., Kikuta, J., Shinozaki, T., Dezawa, K., & Imamura, Y. (2014). Efficacy of distortion correction on diffusion imaging: Comparison of FSL eddy and eddy_correct using 30 and 60 directions diffusion encoding. *Plos One*, 9(11), e112411.
- Yan, C. G., Wang, X. D., Zuo, X. N., & Zang, Y. F. (2016). DPABI: Data processing & analysis for (resting-state) brain imaging. *Neuroinformatics*, 14, 339–351.
- Yoncheva, Y. N., Somandepalli, K., Reiss, P. T., Kelly, C., Di Martino, A., Lazar, M., & Castellanos, F. X. (2016). Mode of anisotropy reveals global diffusion alterations in attention-deficit/hyperactivity disorder. *Journal of the American Academy of Child & Adolescent Psychiatry*, 55(2), 137–145.
- Zhang, Z., Liao, W., Chen, H., Mantini, D., Ding, J. R., Xu, Q., & Jiao, Q. (2011). Altered functional–structural coupling of large-scale brain networks in idiopathic generalized epilepsy. *Brain*, 134(10), 2912–2928.
- Zhao, W., Guo, S., Linli, Z., Yang, A. C., Lin, C. P., & Tsai, S. J. (2020). Functional, anatomical, and morphological networks highlight the role of basal ganglia–thalamus–cortex circuits in schizophrenia. *Schizophrenia Bulletin*, 46(2), 422–431.

Publisher's note Springer Nature remains neutral with regard to jurisdictional claims in published maps and institutional affiliations.

Springer Nature or its licensor (e.g. a society or other partner) holds exclusive rights to this article under a publishing agreement with the author(s) or other rightsholder(s); author self-archiving of the accepted manuscript version of this article is solely governed by the terms of such publishing agreement and applicable law.